of time. Figure 4 shows the results of these measurements. Also plotted are the running totals of light intensity throughout the day. The production of COS in the light bottles followed the light intensity, while dark bottles remained essentially constant at the initial COS concentration. There was essentially no difference between the filtered and unfiltered samples within the experimental uncertainty. The production of COS seems to be due to photooxidation of dissolved organic matter and thus only indirectly related to biological activity. As the 0.45-μm filter will remove all phytoplankton cells, but not all bacteria, a microbial production of COS cannot be rigorously excluded on the basis of this experiment. However, repeated irradiation of seawater with UV light from a small mercury discharge lamp (~400 μW cm^{-2} of 254 nm light) in the presence of dissolved O_2, followed each time by degassing and determination of the COS produced, released COS in slowly decreasing amounts. Under the high UV intensities used, bacteria would have been killed during the first irradiation–degassing cycle and no further COS production should have taken place. UV irradiation of 100 μM solutions of several biochemically relevant organosulphur compounds (cysteine, methionine, glutathione, dimethylpropiothetin) in deionized, distilled water in the same conditions also produced substantial amounts of COS. This reaction did not occur when the solutions were stripped of dissolved O_2 by purging with He before irradiation.

Further evidence for the sea surface being a source of COS to the atmosphere can be seen in the ambient air concentrations measured at the three different locations. At Tallahassee, the mean ambient concentration of COS on 17 January, 18 January, and 18 February 1983 was $\bar{x} \pm s = 515 \pm 82$ p.p.t.v. (parts per 10^{12} by volume) ($n = 28$). This is very close to the mean tropospheric concentration of 512 ± 60 p.p.t.v. reported by Torres *et al.*[3] for a total of 346 measurements during Project GAMETAG. During the period of sampling at the FSU Marine Laboratory, atmospheric concentrations were 537 ± 59 p.p.t.v. ($n = 65$), not significantly different from Tallahassee. However, during the Chesapeake and Delaware Bays cruise, the ambient air concentration was 627 ± 84 p.p.t.v. ($n = 204$), ~20% higher than the continental and coastal concentrations, and may be due to the closer proximity to the surface seawater source. In addition, air concentrations averaged 641 ± 88 p.p.t.v. ($n = 131$) between the hours of 10 am and 8 pm and 601 ± 70 p.p.t.v. ($n = 73$) between 8 pm and 10 am.

Earlier measurements[12,14] in open ocean areas found COS saturation in surface waters averaging approximately 2.0, which results in a flux to the atmosphere of ~0.5–0.9 × 10^{12} g COS yr^{-1}. The higher saturations observed in coastal waters may make the total flux from the oceans greater than previously estimated. We are attempting to gather data from more diverse areas of the ocean to further refine our estimate of this flux.

We thank the captain and crew of the RV *Cape Hatteras* and chief scientist T. R. Fisher for their cooperation. J. T. Byrd and G. Baptist helped with sample collection. This work was supported by NSF grant ATM-8017574.

Received 14 July; accepted 15 September 1983.

1. Crutzen, P. J. *Geophys. Res. Lett.* **3**, 73–76 (1976).
1. Aneja, V. P., Aneja, A. P. & Adams, D. F. *J. Air. Pollut. Control Ass.* **32**, 803–806 (1982).
3. Torres, A. L., Maroulis, P. J., Goldberg, A. B. & Bandy, A. R. *J. geophys. Res.* **85**, 7357–7360 (1980).
4. Turco, R. P., Whitten, R. C., Toon, O. B., Pollack, J. B. & Hamill, P. *Nature* **283**, 283–286 (1980).
5. Crutzen, P. J., Heidt, L. E., Krasnec, J. P., Pollock, W. H. & Seiler, W. *Nature* **282**, 253–256 (1979).
6. Cadle, R. D. *Rev. Geophys. Space Phys.* **18**, 746–752 (1980).
7. Rasmussen, R. A., Khalil, M. A. K., Dalluge, R. W. & Penkett, S. A. *Science* **215**, 665–667 (1982).
8. Carroll, M. A., Heidt, L. E., Cicerone, R. J. & Prinn, R. G. *EOS* **63**, 893 (1982).
9. Turco, R P., Cicerone, R. J., Inn, E. C. Y. & Capone, L. A. *J. geophys. Res.* **86**, 5373–5377 (1981).
10. Sze, N. D. & Ko, M. K. W. *Nature* **280**, 308–310 (1979).
11. Logan, J. A., McElroy, M. B., Wofsy, S. C. & Prather, M. J. *Nature* **281**, 185–188 (1979).
12. Rasmussen, R. A., Khalil, M. A. K. & Hoyt, S. D. *Atmos. Envir.* **16**, 1591–1594 (1982).
13. Johnson, J. E., Harrison, H. & Heidt, L. E. *EOS* **63**, 894 (1982).
14. Ferek, R. J. & Andreae, M. O. *Geophys. Res. Lett.* **10**, 393–396 (1983).
15. Conrad, R., Seiler, W., Bunse, G. & Giehl, H. *J. geophys. Res.* **87**, 8839–8852 (1982).
16. Rasmussen, R. A., Hoyt, S. D. & Khalil, M. A. K. *Chemosphere* **11**, 869–875 (1982).

First observations of the interaction of ocean swell with sea ice using satellite radar altimeter data

C. G. Rapley*

Groupe de Recherche de Géodésie Spatiale,
18 Avenue Edouard Belin, 31055 Toulouse Cedex, France

The action of ocean waves and swell on sea ice in the marginal ice zone (MIZ) controls the size distribution of ice floes and thus affects ice dynamics and the thermodynamics of ice growth and decay. An understanding of ice processes is important because of the influence of the sea-ice cover on high latitude weather and global climate[1]. Also, long-term changes in average sea ice extent could provide a sensitive indication of climatic change if the degree of shorter term variability were better understood[2]. Previous observations of the propagation of swell within the ice pack have been limited in spatial and temporal extent[3–6]. Here we present new results from the US Seasat satellite which suggest that radar altimetry can provide a powerful means of global synoptic monitoring of the interaction between ocean and ice.

The US satellites GEOS-3 and Seasat carried pulse-limited altimeters designed for studies of the geoid and ocean surface[7]. Both instruments obtained data over regions of sea ice. The radar echoes observed were highly variable but were generally stronger and more peaked in time than those from open water[8]. Brown[9] attributes the intense component of first-year ice returns to a coherent signal from smooth ice platelets all lying at the same level amongst the floes. Robin *et al.*[10] show that the peaked component will dominate over the diffuse echo if even as little as 0.01% of the surface contributes a coherent signal. Thus, provided any small areas of new ice or calm water are exposed within the altimeter footprint, we may expect to observe a strong return, and if the sea surface between floes is flat the waveform will be highly peaked.

Figure 1 shows three examples of the evolution of on-board computed values of 'significant wave height' (SWH) and signal strength (automatic gain control, AGC) as the Seasat altimeter passed from open ocean into the ice pack. Obvious features are the step in signal strength at the ice edge (indicated by the arrows) and the greater variability of both parameters over the ice. A particularly interesting feature of the SWH data in Fig. 1*a* and *b* is the gradual overall decline to zero with increasing distance from the ice edge. It is not immediately obvious to what property of the pack ice the SWH value corresponds. An insight into the effect is provided by the altimeter waveform data which typically evolve as shown schematically in Fig. 2 (see also Fig. 1*d*, *e* of Robin *et al.*[10]). Pulse shapes just inside the ice edge (Fig. 2*a*) are often almost identical to those from the nearby ocean, although amplitudes may be as much as 10 times greater. Altimeter pulse risetimes are a measure of the height probability density function of reflecting elements at nadir, and pulse fall times depend on the slope distribution (that is, for specular reflection the maximum duration of the pulse is given by $t_m = (h/c)\theta^2_{max}$ where θ_{max} is the maximum surface slope, and c and h are the velocity of light and satellite altitude respectively). Apparently, neither distribution changes significantly across the ice edge, although the large increase in signal strength implies that the nature of the reflecting elements must alter dramatically. This may be naturally explained if most of the power returned is reflected from thin ice platelets or smooth water between floes as discussed previously. The increasing leading edge slope and more rapid decay of waveforms deeper in the pack (Fig. 2*b*,*c*) then imply a continuous reduction in the interrelated height and slope distributions of the ocean

* Permanent address: Mullard Space Science Laboratory, Department of Physics and Astronomy, University College London, Dorking, Surrey RH5 6NT, UK.

0028-0836/84/020150—03$01.00

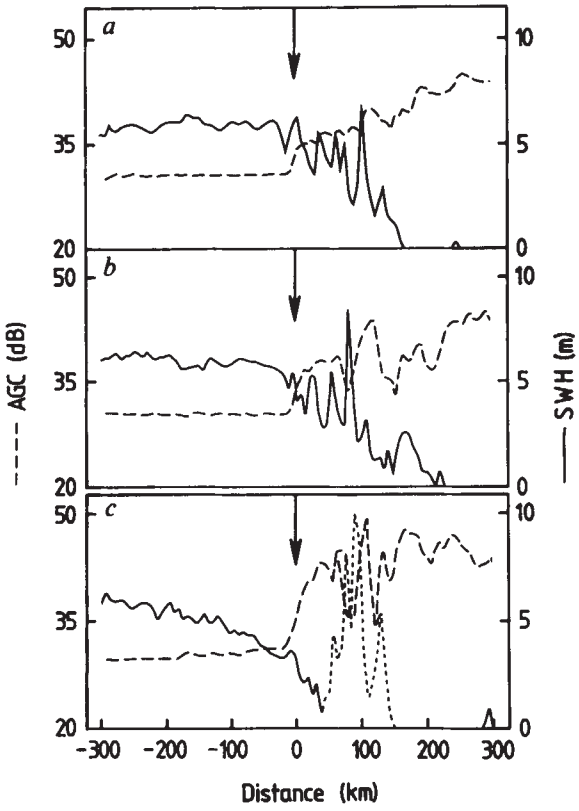

Fig. 1 Three examples of the evolution of on-board computed SWH and AGC values as the Seasat altimeter passed from ocean to sea ice. The ice edge is indicated by the arrow in each case. Note the sudden increase in AGC at the edge and the gradual overall decline of SWH value to zero. Note also the increased SWH noise within the ice pack and the poor data points, particularly in example *c*.

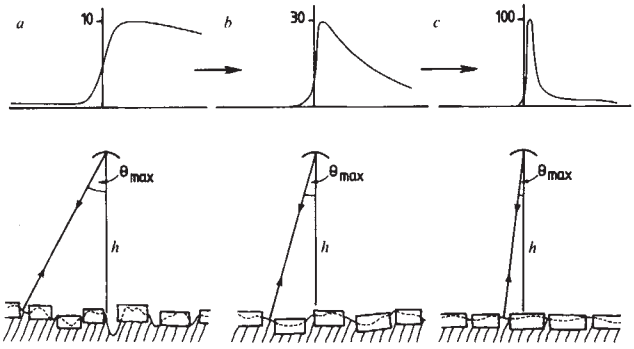

Fig. 2 The evolution of waveform shape and strength as a function of increasing distance into the ice pack. Leading-edge slopes depend on the height distribution of scatterers at nadir just as for ocean returns. Falltimes are determined by the distribution of surface slopes as shown schematically in the lower panels. Pulse strengths are relative to a value unity for a standard ocean return. Pulse shape and strength change as ocean waves and swell are damped out by the action of ice floes within the pack.

(or thin ice) surface as a function of distance from the ice edge. This is consistent with the known behaviour of ocean waves within the ice[5,6].

The relationship between pulse shape and SWH value is not straightforward. The on-board processing methods used by the Seasat altimeter were based on a standard ocean waveform model and the measured instrument performance characteristics[11,12]. An analysis of the response to non-standard pulses is complicated by interactions between all three processing loops[13]. However, an SWH output of zero was special and indicated a value less than the minimum resolvable by the instrument (~40 cm). This could only occur for pulses more peaked than an ocean return, although the degree of 'peakiness' necessary was a function of pulse risetime. Nevertheless, risetime and peakiness are partially interrelated as we have described, and we may therefore use zero SWH as a crude reference level of surface flatness.

Unfortunately, the on-board computed SWH values over sea ice suffered from increased noise and poor data points (note Fig. 1*c* in particular). The latter consist of correlated excursions of the height and SWH signals and resulted from brief attempts by the on-board tracker to follow receding bright features during transitions between areas of high and low surface reflectivity. The effect is similar to that described by Thomas *et al.*[14] for transitions across an ice front. The geographical distribution of extreme events shows a strong concentration in the vicinity of the ice edge and in areas known to be prone to polynya formation, implying an association with transitions from new or first-year ice to open water. Alternatively, 'hunting' by the on-board tracker when processing highly peaked pulses[13] could have introduced similar errors. Occurrences within the ice pack were more frequent towards the coast where AGC values were low, and may have resulted from transitions to areas of continuous ice or snow cover. Much of the contaminated data can be recovered by analysis of the altimeter waveforms but this represents a very major computing task. Thus, an exploratory investigation of swell propagation within the ice was carried out using the SWH data, recognizing its limitations. The use of a spatial resolution of ~70 km (10 point averages) and the averaging effect of adjacent groundtracks reduced the impact of data contamination on the results.

Figure 3 shows data from four successive repeats of the 3-day orbit cycle executed by Seasat during September 1978 at the time of maximum sea ice extent. The ice edge derived using an AGC threshold of 33 dB and the zero SWH contour are shown, the region between being shown as solid areas. Despite the coarse spatial resolution used, inconsistencies in the location of the ice edge occur due to motion within a 3-day cycle. These are represented by small re-entrant features. The SWH contour joins locations at which zero SWH is first encountered on entry into the ice pack. All non-zero SWH values within this contour are ignored as are occasional groundtracks obviously affected by poor data. Also shown are zones of high ocean swell (>5 m) derived using the method of Mognard[15] (see also ref. 16). The zones shown represent major storm systems. An immediate qualitative correspondence can be seen between areas in which the zero SWH contour is furthest from the ice edge and nearby zones of high swell. Furthermore, changes in the width of the band follow the temporal and spatial evolution of the swell storms. For example, the sector between 30° E and 60° W contains little swell storm activity and consistently exhibits a narrow band of swell penetration, whereas the decay of the major swell storm between 30° E and 120° E is matched by a decline in penetration distance.

The altimeter data therefore provide a means of using the ice as a detector of swell or, alternatively, the swell as a probe of the ice. The energy decay of each swell component is known to be exponential with an attenuation coefficient strongly dependent on swell wavelength and ice thickness[5,6]. The width of the band shown here also depends on the amplitude of the penetrating component at the ice edge and may be affected by the inadequacies of the SWH data as described above. Nevertheless, the observed penetration distances of up to 300–400 km are consistent with previous *in situ* measurements[3]. Detailed, quantitative studies will require analysis of the waveform data. Even so, the SWH data provide useful qualitative insights into ice properties. For example, the strong propagation of low swells into the edge features seen between 30° W and 90° W in Fig. 3*a* and at 30° W in Fig. 3*d*, implies that the ice is thin, as does their rapid spatial variability.

In an attempt to relate swell effects to ice edge growth, Fig. 4 shows a detail of ice edge changes over the four periods. A good general correlation is observed between ice edge variability and regions affected by swell, particularly in the case of the

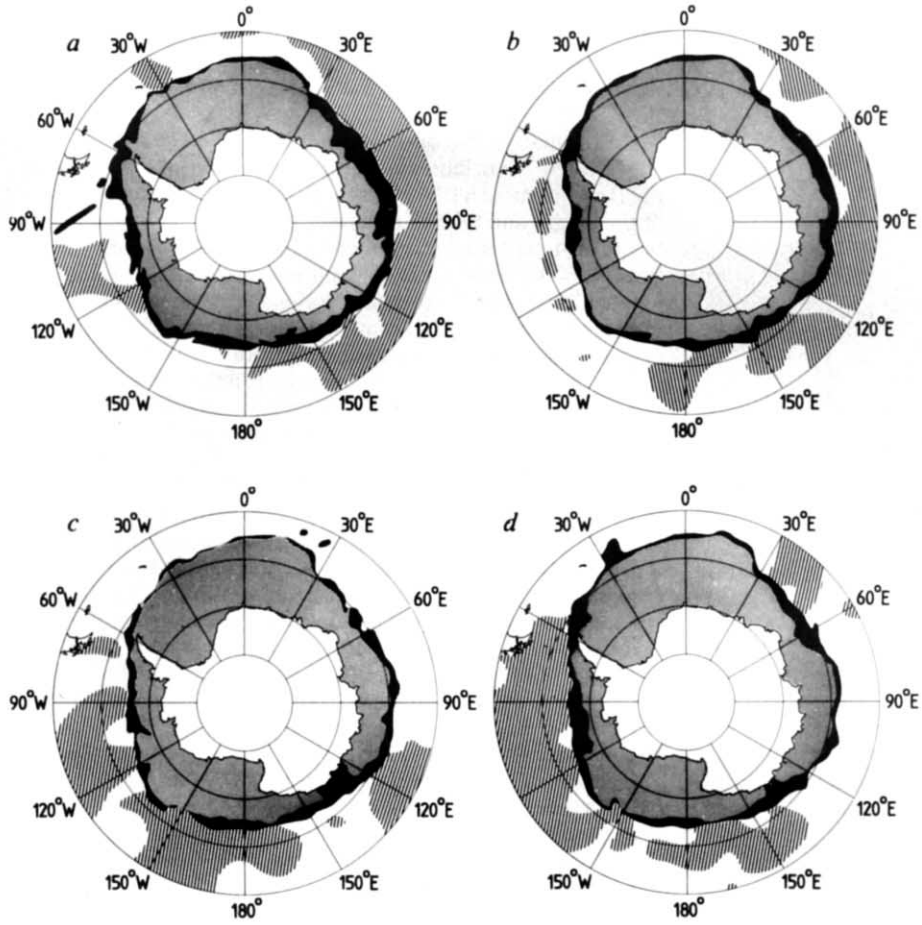

Fig. 3 Four consecutive 3-day maps of Antarctic sea ice (shaded areas) and regions of ocean swell greater than 5 m (cross-hatched areas) during September 1978. Zones of swell penetration into the ice (solid areas) derived from the SWH data contract and expand with the decline and subsequent growth of nearby ocean swell storms. Note the generally limited penetration in the region 30° E to 60° W where swell activity is low during this period, other than the feature suspected to consist of thin ice in *d*.

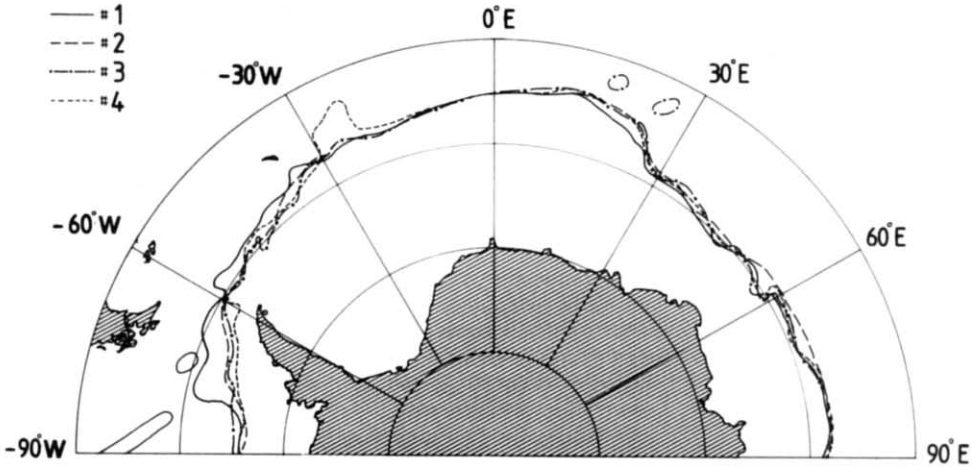

Fig. 4 Detail of the ice-edge variations over the four 3-day cycles. Greater variability occurs in regions affected by swell. Features showing the greatest changes are deeply penetrated by low-amplitude swells (see Fig. 3) implying that the ice is comparatively thin.

(apparently) thin ice features already noted. Keliher[17] has previously reported an association between pack ice disturbances and regions of high sea state.

We may conclude, therefore, that variations in altimeter return pulse shape provide a powerful means of monitoring swell propagation within the ice pack. Difficulties associated with the use of on-board SWH values have important implications on instrument design and data analysis procedures for future satellite altimeter missions.

I thank the Centre Nationale d'Etudes Spatiales, France for financial support and the Groupe de Recherche de Géodésie Spatiale for their hospitality and assistance. I am particularly grateful to Mr Claude Brossier for his hard work and enthusiasm in producing the data plots and to Dr Michel Lefebvre for his encouragement. I acknowledge useful discussions with Drs Nelly Mognard and Bill Campbell.

Received 19 September; accepted 28 October 1983.

1. Committee on Glaciology, Polar Research Board *Snow and Ice Research, An Assessment* (National Academy Press, Washington DC, 1983).
2. Zwally, H. J., Parkinson, C. L. & Comiso, J. C. *Science* **220,** 1005–1012 (1983).
3. Robin, G. de Q. *Phil. Trans. R. Soc.* **A255,** 313–339 (1963).
4. Wadhams, P. *J. geophys. Res.* **80,** 4520–4528 (1975).
5. Wadhams, P. *Deep Sea Res.* **25,** 23–40 (1978).
6. Squire, V. A. & Moore, S. C. *Nature* **283,** 365–368 (1980).
7. Townsend, W. F. *IEEE J. Oceanic Engng* **OE-5**(2), 80–92 (1980).
8. Dwyer, R. E. & Godin, R. H. *NASA Contract Report* 156862 (1980).
9. Brown, G. S. *Radio Sci.* **17,** 233–243 (1982).
10. Robin, G. de Q., Drewry, D. J. & Squire, V. A. *Phil. Trans. R. Soc.* **A309,** 447–463 (1983).
11. MacArthur, J. L. *Proc. Oceans-76, MTS-IEEE* 1–8 (1976).
12. MacArthur, J. L. *Applied Physics Laboratory,* SDO-5232 (Johns Hopkins University, 1978).
13. Rapley, C. G. *et al. ESA Contract Report* 5182/82/F/CG(SC) (1983).
14. Thomas, R. H., Martin, T. V. & Zwally, J. H. *Ann. Glaciol.* (in the press).
15. Mognard, N. thesis, Univ. Paul Sabatier de Toulouse (1982).
16. Mognard, N., Campbell, W. J., Cheny, R. E. & Marsh, J. G. *J. geophys. Res.* **88,** 1736–1744 (1983).
17. Keliher, T. E. *AIDJEX Bull.* **34,** 114–135 (1976).